Preprints of the 21st IFAC World Congress (Virtual)
Berlin, Germany, July 12-17, 2020

Amplitude Design of Perturbation Signal in Frequency-Domain Analysis of Grid-Connected Systems

Henrik Alenius * **Roni Luhtala** ** **Tomi Roinila** *

* *Faculty of Information Technology and Communication Sciences, Tampere University, Finland, (e-mail: henrik.alenius@tuni.fi; tomi.roinila@tuni.fi).*
** *Faculty of Engineering and Natural Sciences, Tampere University, Finland, (e-mail: roni.luhtala@tuni.fi).*

Abstract: The rise of renewable electricity production has driven the power grid to a remarkable transformation, where a large share of the electricity production is integrated to the grid through power-electronic inverters. The inverters have fast internal dynamics and no inherent inertia, which makes the power grid prone to stability issues. The stability analysis to ensure system robustness can be performed based on the impedance ratio of the inverter and power grid. The grid impedance is often an unknown parameter, and methods for grid impedance measurements are required. Past studies have presented a number of measurement methods based on a broadband perturbation, such as pseudo-random binary sequence (PRBS), and Fourier techniques for obtaining the grid impedance. However, only a little attention has been paid to the injection-amplitude design, and most often, the amplitude has been selected based on trial and error. This work presents an algorithm based on the total harmonic distortion (THD) levels of grid currents and voltages for choosing a suitable perturbation amplitude. The proposed method makes it possible to fully automate the stability analysis of a grid-connected system. Experimental results based on a three-phase grid-connected inverter are presented and used to demonstrate the effectiveness of the proposed method.

Keywords: Power Electronics, Grid-Connected Systems, Frequency-Response Measurements, Broadband Sequences, Perturbation Design, Excitation Amplitude.

1. INTRODUCTION

The rise of renewable electricity production has started to change the power grid (Bose (2013)). Unlike conventional centralized synchronous generators, the renewable energy production is often distributed in the system. Additionally, the majority of wind and solar power is interfaced to the grid through a grid-connected three-phase inverter, which accommodates the produced power to the grid frequency and voltage. Fig. 1 presents a schematic of an inverter interfacing a renewable power source to the grid. The inverters typically have fast internal dynamics and no inherent inertia, which makes the system prone to stability issues. One issue that has been studied is the harmonic resonance between the inverter and power grid, which occurs in systems that have high penetration of grid-connected inverters (Li (2017); Liu et al. (2017)). The harmonic resonance may appear to be a power quality problem, but it is actually an indication of lack of system stability margin and may lead to instability and disruption of inverter operation if the grid impedance or the inverter power level further increases.

Recent studies have presented multiple methods for stability analysis of grid-connected inverters (Sun (2011); Amin and Molinas (2017); Wang et al. (2017b,a); Rygg and Molinas (2017); Alenius et al. (2019a,b)). The most applied approach is the impedance-based stability criterion, which analyzes the inverter output impedance and grid impedance at the common interface, where a Nyquist stability criterion is applied to the ratio of these impedances (Sun (2011); Suntio et al. (2019); Alenius and Roinila (2020)). In general, the inverter impedance can be obtained by impedance modeling (Wang et al. (2018)). However, the grid impedance seen from the interface is often either unknown or highly complex and, therefore, difficult to model. Thus, in many cases the grid impedance is a black-box model and accurate analysis requires measurements or estimates. Additionally, the grid conditions may fluctuate along with system power flows, which affects the impedance (Jessen et al. (2015)). The grid impedance is a crucial variable as the stability issues emerge mostly in high-impedance grids typical for remote locations or systems that have high penetration of distributed generation.

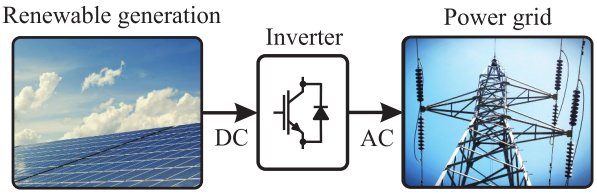

Fig. 1. Power-electronic interface between renewable generation and power grid.

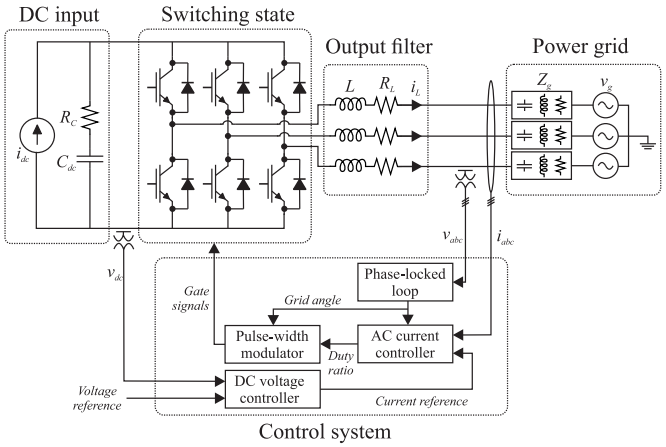

Fig. 2. Three-phase grid-connected inverter.

Recently, a number of measurement techniques for obtaining the grid impedance for stability analysis have been presented (Cespedes and Sun (2013); Roinila et al. (2018); Luhtala et al. (2020)). In most of the presented methods, a current excitation is applied to perturb the system. In grid impedance measurements, the excitation can be injected to the current references of a grid-connected inverter, and the currents and voltages are measured from the output terminals of the inverter. The frequency response of the impedance can be obtained by applying Fourier methods to these currents and voltages. Broadband signals have become popular for excitation as they allow measurements from multiple frequencies simultaneously, resulting in significantly shorter measurement times in comparison to conventional sine sweep (Godfrey (1993); Roinila et al. (2018)). Particularly attractive characteristics have been demonstrated in pseudo-random binary sequences (PRBS), which have tunable frequency spectrum, minimal crest factor, and they are easy to generate. In addition, the signals are periodic, which allows averaging over multiple periods to increase the signal-to-noise ratio (SNR).

One of the challenges of the previously presented measurement techniques of the grid impedance has been the selection of the excitation amplitude. The excitation amplitude determines the SNR in the measurements, and a sufficiently large amplitude is required to overcome the noise in the system. On the other hand, the excitation appears as harmonic pollution in the power grid, and too large excitation amplitude may trigger system nonlinearities. Consequently, the amplitude should be selected as a tradeoff between these two colliding requirements. While previously introduced methods have been able to measure the grid impedance accurately, the excitation amplitude has been often selected by trial and error, and no straightforward guidelines or methods have been presented for the amplitude selection. The lack of methods for simple/automated amplitude selection not only increases the total measurement time for obtaining the impedance, but also affects the measurement quality as the system parameters typically vary over time and, therefore, a varying value for the amplitude may be required.

This work presents a method for amplitude selection for impedance measurements of grid-connected systems. The proposed method considers the effect of perturbation injection on grid-side voltage and current total harmonic distortion (THD), and tunes the amplitude with respect to the THD limits. The impact of averaging and amplitude selection on measurement accuracy is demonstrated for grid-impedance measurements applying a grid-connected inverter. Experimental power hardware-in-the-loop (PHIL) measurements are performed with a 2.7 kW three-phase inverter for grids with varying impedance.

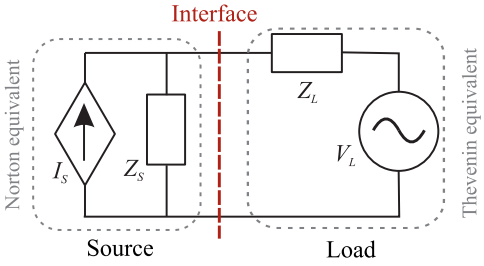

Fig. 3. Equivalent source-load model of grid-connected inverter.

The remainder of the paper is organized as follows. Section II presents the impedance-based stability criterion for grid-connected inverter. Section III considers system identification with maximum-length binary sequence (MLBS) and presents the proposed algorithm for injection amplitude selection. In Section IV, the experimental setup and measurement results are shown. Section V discusses the use of the proposed method and suggests general guidelines for the amplitude selection. Finally, conclusions are drawn in Section VI.

2. IMPEDANCE-BASED STABILITY CRITERION

Fig. 2 shows a simplified diagram of a grid-connected three-phase inverter. The system can be analyzed as a simplified source-load equivalent, where the inverter represents a source and the grid acts as a load, as shown in Fig. 3. The source is modeled by a Norton equivalent circuit, as a current source I_S in parallel with the source impedance Z_S. The load voltage is denoted by V_L, and the load impedance by Z_L. Assuming the source is stable when unloaded and the load is stable when powered by an ideal source, the stability and other dynamic characteristics of the interconnected system can be determined from the transfer function

$$G(s) = \frac{1}{1 + Z_\mathrm{L}(s)/Z_\mathrm{S}(s)} \tag{1}$$

where $Z_\mathrm{L}(s)$ is the load impedance and $Z_\mathrm{S}(s)$ is the source impedance. The impedance ratio $Z_\mathrm{L}(s)/Z_\mathrm{S}(s)$ must satisfy Nyquist criterion for the system to be stable (Sun (2011)). For three-phase devices, similar analysis can be performed applying impedance matrices, for example in dq frame, and generalized Nyquist criterion (GNC) applicable for multi-input-multi-output (MIMO) systems (Belkhayat (1997)). The source impedance of an inverter can be acquired from small-signal model, data sheet, or by measurements from output terminals. The load impedance (grid impedance), however, is typically unknown and can vary over a wide range. Thus, the grid impedance measurements are often required for stability analysis of grid-connected devices.

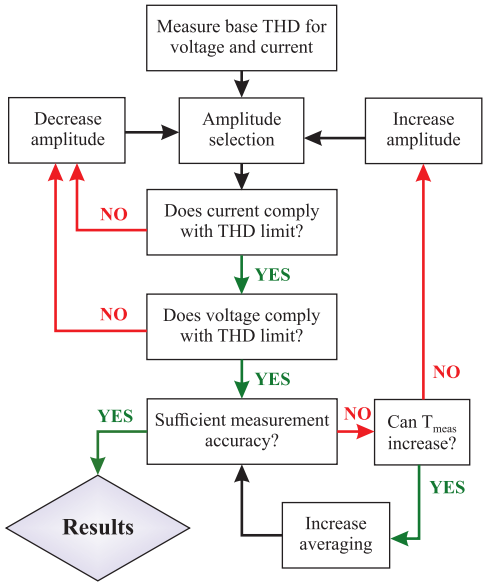

Fig. 4. Flowchart of the amplitude selection algorithm.

3. BROADBAND SYSTEM IDENTIFICATION

In steady state, a grid-connected system can be considered as a linear time-invariant system for small disturbances. According to basic control theory, such system can be fully characterized by its impulse response in the time domain, which can be transformed to the frequency domain and presented as a frequency-response function (Godfrey (1993)). A method to obtain the frequency-response function of the grid impedance is to apply a broadband perturbation such as the pseudo-random binary sequence (PRBS). In the method, the perturbation is injected into the network (for example, by using the inverter), and Fourier analysis is applied to extract the frequency-domain voltages and currents to obtain the impedance.

3.1 Maximum-Length Binary Sequence

Maximum-length binary sequence (MLBS) is a type of pseudo-random sequence that has been successfully applied in grid-impedance measurements (Roinila et al. (2018)). The MLBS has multiple characteristics that are suitable for identification of grid-connected systems; it has a largely adjustable frequency spectrum for both bandwidth and resolution, and its binary nature results in an ideal crest factor. Additionally, binary sequences are easy to generate and inject using switched-mode devices, and the periodic sequences can be averaged over arbitrary number of periods.

The MLBS is deterministic and periodic over sequence length N, which can be chosen freely for $N = 2^n - 1$, where n is an integer. The sequence can be easily generated by a XOR-feedback shift register, which produces a binary signal between 0 and 1 repeating after N steps. In order to produce a symmetrical excitation that has average close to zero, the injection is usually mapped to vary between -1 and 1. The amplitude of the injection can be chosen freely, and it is a trade-off between measurement accuracy and system disturbance. The measurement time for P averaged periods is given as

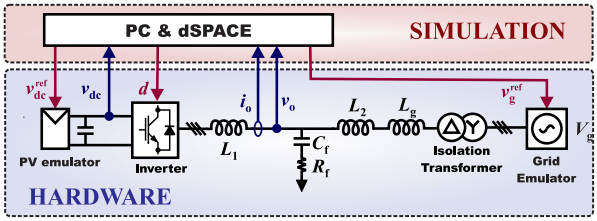

Fig. 5. Experimental PHIL setup schematic diagram.

$$T_{\text{meas}} = NP/f_{\text{gen}} \tag{2}$$

where f_{gen} is the generation frequency. In this work, a logarithmic averaging is applied (Pintelon and Schoukens (2001)), where the measured signal is averaged based on

$$X(j\omega) = \left(\prod_{k=1}^{P} x_{\text{k}}(j\omega) \right)^{(1/P)} \tag{3}$$

where $x_{\text{k}}(j\omega)$ is a signal in frequency domain. The logarithmic averaging reduces the uncorrelated noise in the measurements to the power of $x^{(1/P)}$.

3.2 Design of Injection Amplitude

The selection of the injection amplitude plays important role in the grid-impedance measurement, particularly in online applications where the impedance is measured in real time. The amplitude must be high enough in order to provide good signal-to-noise ratio (SNR) but low enough to avoid too high nonlinear distortions.

In this work, the value of total harmonic distortion (THD) is used as an indicator for iteratively selecting the appropriate injection amplitude. The THD is the most used indicator for power quality, and consequently, standards and regulations have been widely imposed on THD values of grid currents and voltages. As the excitation signal from the inverter inevitably distorts the currents and voltages in the grid, the THD can be applied as a feedback for the amplitude selection.

Fig. 4 presents the suggested amplitude selection algorithm as a flowchart, where the injection amplitude is tuned iteratively. The THD limits for currents and voltages can either be set by a standard, or by the user. The selection depends on the application and the base THD level, and the designer of a grid-connected system usually has good insight on the desired THD. The algorithm prioritizes amplitude selection over averaging, so the injection amplitude is increased to the THD limit first, and then if necessary, the number of averaged periods is increased. If a sufficient measurement accuracy is not met even with maximum allowable injection amplitude and measurement time, one of the requirements must be loosened until sufficient accuracy is met.

4. EXPERIMENTS

The experiments are performed with a power hardware-in-the-loop (PHIL) setup, where a kW-scale three-phase inverter (*Myway Plus MWINV-9R144*) is connected to a linear voltage amplifier (*Spitzenberger & Spies PAC 15000*) that emulates three-phase grid voltages. A real-time simulator (*dSPACE model 1103*) provides the voltage references for the voltage amplifier. In addition, the

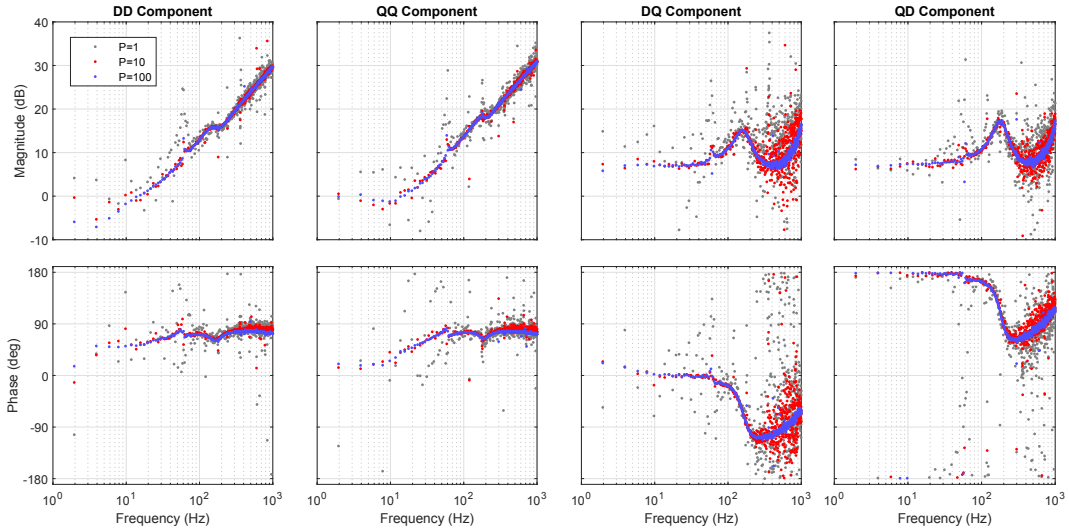

Fig. 6. Measured MIMO impedance with either 1, 10, or 100 averaged periods.

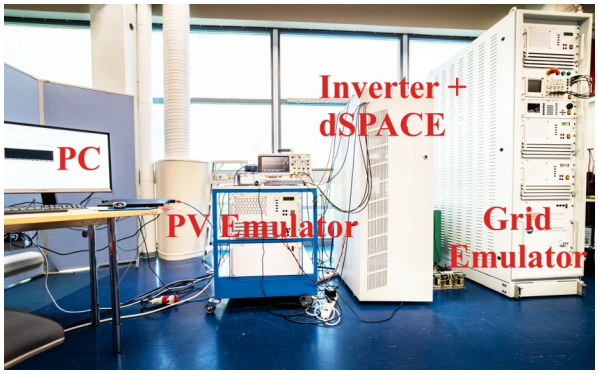

Fig. 7. Picture of the laboratory setup.

inverter control scheme is implemented on the dSPACE, which produces the driving gate signals for the IGBT switches in the inverter. A photovoltaic emulator (*Spitzenberger & Spies PVS 7000*) provides the DC input power for the inverter by emulating the voltage-current profile of a photovoltaic system. An external hardware inductor and isolation transformer are connected between the inverter and the voltage amplifier (grid emulator), which here act as the grid impedance. Fig. 5 presents a block diagram of the experimental setup, and a picture of the setup is shown in Fig. 7.

The experiments consist of grid-impedance measurements performed with the grid-connected inverter. The MLBS excitation signal is added to the current references of the inverter current controller, so the inverter produces a current-type injection to the system. The three-phase currents and voltages are measured from the output terminal of the inverter, and these measurements are applied in the grid-impedance measurements. These measurements are required also for the control system, so no additional sensors are required. The current and voltage quality are assessed from these measurements in both time domain (waveforms) and frequency domain (THD and power spectrum). The measurements are performed for three different grid impedances; in addition to the isolation transformer, the grid connection had either no additional impedance, a 4 mH inductor, or a 9 mH inductor. The corresponding short-circuit ratios (SCR) are 22, 7.1, and 3.9, respectively. The grid with lowest impedance (highest SCR) represents a robust grid where stability issues are rare, and the highest impedance grid (lowest SCR) corresponds to a high-impedance system prone to stability issues. In order to obtain the full-order impedance in the dq-domain, two separate measurements are performed to different channels (d-injection yields dd- and dq-components, q-injection yields qq- and qd-components).

4.1 Impedance Measurements

In practice, a high-resolution broadband measurement requires averaging over multiple periods in order to increase the SNR to a sufficient level. In this work, the maximum number of averaged periods for each measurement is 100. Fig. 6 presents the measured impedances from the SCR = 22 grid, and shows the results with logarithmic averaging over different number of periods with excitation amplitude of 3 % of nominal current (approximately 300 mA). It is apparent that with low number of averaged periods, the measurements are noisy, and especially the crosscouplings (QD and DQ) are very scattered due to low magnitude. However, increasing the averaging to 10 periods already illustrates the shape of the impedance accurately. With 100 averaged periods, the measurements can be applied for example in impedance-based analysis without considerable loss of accuracy. In all measurements, the frequencies closest to the fundamental frequency (60 Hz) are corrupted by the fundamental currents and voltages.

Another approach to enhance the measurement accuracy is to increase the excitation amplitude, which results in higher SNR. However, in online measurements the excitation pollutes the grid currents and voltages increasing the system THD. Although the perturbation is injected as a current excitation, it depends on the grid impedance whether currents or voltages are more corrupted. In strong grids (low impedance), the grid voltages remain ideally uncorrupted as the current produces insignificant voltage response in low grid impedance. In weak grids (high

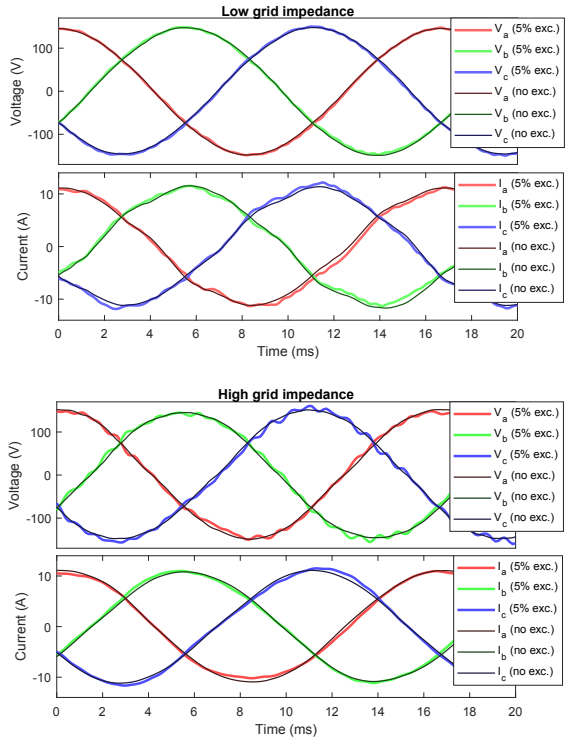

Fig. 8. Time-domain currents and voltages with no excitation and 5% excitation in strong grid (upper) and in weak grid (lower).

impedance), on the other hand, the current produces larger voltage response. However, as the grid impedance is typically inductive, it increases the filtering effect resulting in smoother current waveforms. Consequently, the perturbation corrupts the current THD in strong grids and the voltage THD in weak grids. Fig. 8 shows the measured three-phase time-domain currents and voltages in two cases; in strong grid connection (upper, SCR = 22) and in weak grid connection (lower, SCR = 3.9). In both experiments, the injection amplitude was 5 % of the nominal current. Table 1 presents the measured current and voltage THDs in grids with different impedances for five different injection amplitudes. Based on the table, the following conclusions can be given

- low grid impedance results in high current THD and low voltage THD
- high grid impedance results in low current THD and high voltage THD
- excitation amplitude below 1 % has no effect on current or voltage THD (in these systems)
- even 5 % excitation has a moderate effect on the THD (in these systems).

4.2 Measurement Variance

The quality of the measurements can be characterized by measurement variance to reference. In this case, no analytical reference is available, so the reference is constructed from the measurement with maximum averaging and excitation amplitude by fitting a transfer function to the obtained data. The variance is given by

Table 1. Measured THD values of currents and voltages.

	Injection amplitude					
	0.0 %	0.5 %	1.0 %	3.0 %	5.0 %	
0 mH	5.41 %	5.42 %	5.47 %	6.03 %	7.03 %	Current
4 mH	2.91 %	2.90 %	2.96 %	3.50 %	4.41 %	
9 mH	2.15 %	2.15 %	2.19 %	2.70 %	3.54 %	
0 mH	1.17 %	0.99 %	1.11 %	1.42 %	1.29 %	Voltage
4 mH	2.02 %	1.94 %	2.05 %	2.33 %	3.21 %	
9 mH	2.38 %	2.45 %	2.17 %	2.99 %	3.74 %	

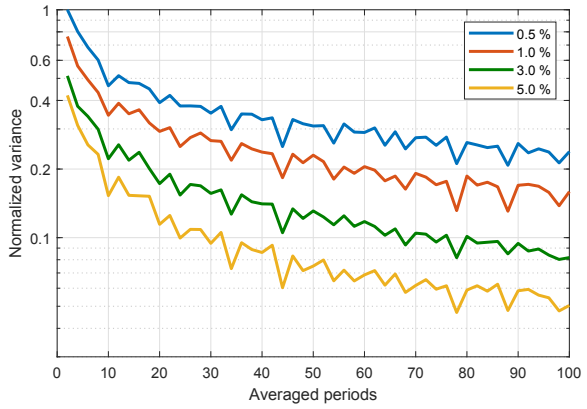

Fig. 9. Measurement variance as a function of number of averaged periods.

$$\sigma^2 = \sum_{f=1}^{f_{\max}} [Z_{\text{fit}}(f) - Z(f)]^2 \tag{4}$$

where $Z_{\text{fit}}(f)$ is the fitted impedance and $Z(f)$ is the measured impedance. The total variance of the measurement is the sum of component variances. To illustrate the impact of both amplitude and averaging, Fig. 9 shows the variance from reference as a function of number of averaged periods for different excitation amplitudes, measured from the strongest grid. The variance is normalized, where the variance is compared to measurement that has the highest variance. The figure shows a clear increase in measurement quality when the excitation amplitude is increased, and on the other hand, when the number of averaged periods increases. Based on the trends shown in the figure, it is apparent that lower injection amplitude can be compensated only partially by increasing the averaging. This supports the proposed algorithm, where the injection amplitude is increased to the THD limit first.

5. DISCUSSION

A proper amplitude design requires thorough consideration of the desired measurement accuracy, grid under measurement, and base level of the THD for grid voltages and currents. Sufficient measurement accuracy can be obtained with small excitation amplitude by allowing long measurement time for averaging over multiple periods. Yet, increase in excitation amplitude is shown to enhance the measurement accuracy, which can not be achieved by simply increasing the averaging and measurement time. Fig. 10 illustrates the inherent trade-offs between measurement quality (indicated by SNR) against grid THDs and

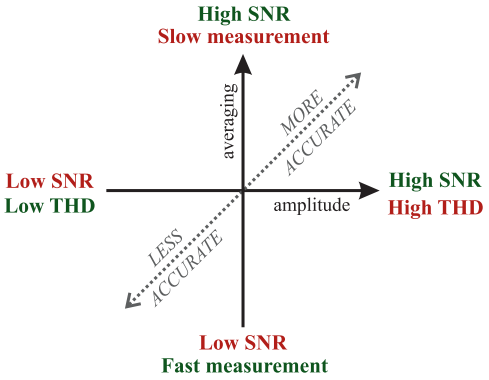

Fig. 10. Inherent trade-offs in measurement accuracy.

measurement duration. The optimal perturbation design depends on the application and grid conditions, and a generalized optimal design can not be derived. However, the proposed algorithm can be utilized as a procedure to find a design that optimizes the amplitude and averaging to a specific application.

6. CONCLUSION

Wideband identification methods based on broadband perturbation and Fourier techniques have become popular in stability analysis of grid-connected systems. This work has presented a method for tuning the perturbation amplitude and measurement duration with respect to the given limitations in grid-side THD levels. In impedance measurements of grid-connected systems, the perturbation signal pollutes the grid currents and voltages with harmonic content. Consequently, the perturbation amplitude should be designed carefully to provide sufficient signal-to-noise ratio and to minimize the disturbance to normal system operation. This work has illustrated the impact of perturbation amplitude on measurement accuracy and grid current and voltage total harmonic distortions in impedance measurements of grid-connected systems. Experimental results based on a three-phase grid-connected inverter operating under varying conditions were shown to demonstrate the proposed method.

REFERENCES

Alenius, H., Berg, M., Luhtala, R., and Roinila, T. (2019a). Stability and Performance Analysis of Grid-Connected Inverter Based on Online Measurements of Current Controller Loop. In *Proc. Industrial Electronics Conference (in press)*, 7 pages.

Alenius, H., Berg, M., Luhtala, R., Roinila, T., and Messo, T. (2019b). Impedance-Based Stability Analysis of Multi-Parallel Inverters Applying Total Source Admittance. In *Proc. 20th Workshop on Control and Modeling for Power Electronics (COMPEL)*, 8 pages.

Alenius, H. and Roinila, T. (2020). Impedance-Based Stability Analysis of Paralleled Grid-Connected Rectifiers: Experimental Case Study in a Data Center. *Energies*, 13(2109). doi:10.3390/en13082109.

Amin, M. and Molinas, M. (2017). Small-Signal Stability Assessment of Power Electronics based Power Systems: A Discussion of Impedance- and Eigenvalue-based Methods. *IEEE Transactions on Industry Applications*, 53(5), 5014–5030.

Belkhayat, M. (1997). *Stability criteria for AC power systems with regulated loads*. Doctoral thesis, Purdue University.

Bose, B. (2013). Global Energy Scenario and Impact of Power Electronics in 21St. Century. *IEEE Transactions on Industrial Electronics*, 60(7), 2638–2651.

Cespedes, M. and Sun, J. (2013). Three-phase impedance measurement for system stability analysis. *Proc. IEEE 14th Workshop on Control and Modeling for Power Electronics (COMPEL)*, 6 pages.

Godfrey, K. (1993). *Perturbation Signals for System Identification*. Prentice Hall, UK.

Jessen, L., Gunter, S., Fuchs, F.W., Gottschalk, M., and Hinrichs, H.J. (2015). Measurement results and performance analysis of the grid impedance in different low voltage grids for a wide frequency band to support grid integration of renewables. In *Proc. IEEE Energy Conversion Congress and Exposition*, 1960–1967.

Li, C. (2017). Unstable Operation of Photovoltaic Inverter from Field Experiences. *IEEE Transactions on Power Delivery*, 33, 1013–1015.

Liu, H., Xie, X., He, J., Xu, T., and Yu, Z. (2017). Subsynchronous Interaction Between Direct-Drive PMSG Based Wind Farms and Weak AC Networks. *IEEE Transactions on Power Systems*, 32(6), 4708–4720.

Luhtala, R., Alenius, H., Messo, T., and Roinila, T. (2020). Online Frequency Response Measurements of Grid-Connected Systems in Presence of Grid Harmonics and Unbalance. *IEEE Transactions on Power Electronics*, 35(4), 3343–3347.

Pintelon, R. and Schoukens, J. (2001). *System Identification - A Frequency Domain Approach*. John Wiley & Sons.

Roinila, T., Messo, T., and Santi, E. (2018). MIMO-identification techniques for rapid impedance-based stability assessment of three-phase systems in DQ Domain. *IEEE Transactions on Power Electronics*, 33(5), 4015–4022.

Rygg, A. and Molinas, M. (2017). Apparent impedance analysis: A small-signal method for stability analysis of power electronic-based systems. *IEEE Journal of Emerging and Selected Topics in Power Electronics*, 5(4), 1474–1486.

Sun, J. (2011). Impedance-based stability criterion for grid-connected inverters. *IEEE Transactions on Power Electronics*, 26(11), 3075–3078.

Suntio, T., Messo, T., Berg, M., Alenius, H., Reinikka, T., Luhtala, R., and Zenger, K. (2019). Impedance-Based Interactions in Grid-Tied Three-Phase Inverters in Renewable Energy Applications. *Energies*, 12(464).

Wang, X., Harnefors, L., and Blaabjerg, F. (2018). Unified Impedance Model of Grid-Connected Voltage-Source Converters. *IEEE Transactions on Power Electronics*, 33(2), 1775–1787.

Wang, Y., Wang, X., Blaabjerg, F., and Chen, Z. (2017a). Harmonic instability assessment using state-space modeling and participation analysis in inverter-fed power systems. *IEEE Transactions on Industrial Electronics*, 64(1), 806–816.

Wang, Y., Wang, X., Blaabjerg, F., and Chen, Z. (2017b). Small-Signal Stability Analysis of Inverter-Fed Power Systems Using Component Connection Method. *IEEE Transactions on Smart Grid*, 9(5), 5301–5310.